Direct dating of mid-crustal shear zones with synkinematic allanite: new in situ U-Th-Pb geochronological approaches applied to the Mont Blanc massif

Bénédicte Cenki-Tok, James R. Darling, Yann Rolland, Bruno Dhuime, Craig D. Storey

Terra Nova

Direct dating of mid-crustal shear zones with synkinematic allanite: New in-situ U-Th-Pb geochronological approaches applied to the Mont Blanc massif

Journal:	*Terra Nova*
Manuscript ID:	TER-2012-0113.R2
Wiley - Manuscript type:	Paper
Date Submitted by the Author:	n/a
Complete List of Authors:	Cenki-Tok, Bénédicte; Géosciences Montpellier, Darling, James; University of Portsmouth, Rolland, Yann; Géosciences Azur, Dhuime, Bruno; University of Bristol, Storey, Craig; University of Portsmouth,
Keywords:	allanite, U-Th-Pb geochronology, shear zones, Mont Blanc massif

Direct dating of mid-crustal shear zones with synkinematic allanite: New *in situ* U-Th-Pb geochronological approaches applied to the Mont Blanc massif

Bénédicte Cenki-Tok[1,2*], James R. Darling[3,4*], Yann Rolland[5], Bruno Dhuime[6], and Craig D. Storey[4]

[1] Université Montpellier 2, Géosciences Montpellier, UMR5243, Place Eugène Bataillon, 34095 Montpellier

[2] Institute of Geological Sciences, Baltzerstrasse 1+3, University of Bern, CH-3012 Bern, Switzerland

[3] Department of Earth Sciences, University of Western Ontario, 1151 Richmond Street North, London, Ontario, Canada, N6A 5B7

[4] Crustal Evolution Research Group, School of Earth and Environmental Sciences, University of Portsmouth, Burnaby Building, Burnaby Road, Portsmouth, PO1 3QL, UK

[5] Géoazur, UMR 7329, Université de Nice Sophia Antipolis, CNRS, IRD, 28 Av. de Valrose, BP 2135, 06108 Nice, France.

[6] Department of Earth Sciences, University of Bristol, Wills Memorial Building, Queen's Road, Bristol BS8 1RJ, UK

* Correspondence: benedicte.cenki-tok@gm.univ-montp2.fr or james.darling@port.ac.uk

ABSTRACT

Dating the timing of motion on crustal shear zones is of tremendous importance for understanding the assembly of orogenic terranes. This objective is achieved in this paper by combining petrological and structural observations with novel developments in *in situ* U-Th-Pb geochronology of allanite. A greenschist facies shear zone within the Mont Blanc Massif is documented. Allanite is synkinematic and belongs to the mylonitic assemblage. LA-ICP-MS U-Th-Pb isotope analyses of allanite reveal high contents and highly radiogenic isotopic compositions of the common-Pb component. The use of measured Pb-isotope compositions of associated minerals (feldspars and chlorite) is critical for

accurate common-Pb correction, and provides a powerful mechanism for linking allanite growth to the metamorphic assemblage. A mean $^{208}Pb/^{232}Th$ age of 29.44 ± 0.95 Ma is accordingly taken for synkinematic allanite crystallisation under greenschist facies conditions. This age reflects the timing of the Mont Blanc underthrusting below the Penninic Front and highlights the potential of directly dating deformation with allanite.

Introduction

Resolving the timing and rates of crustal deformation is fundamental to our understanding of tectonic and orogenic processes. Direct dating of deformation features by isotopic techniques has great potential to provide new insights into the complexities of orogenesis and tectonics in general. Of particular interest are shear zones, which can accommodate vast lateral and vertical crustal motions, control the development of tectonic features, and provide important pathways for orogenic and ore-forming fluids.

In contrast to constraining deformation ages through cross-cutting structural relationships, the direct-dating approach focuses upon isotopic analysis of synkinematic minerals that belong to the metamorphic assemblage associated with deformation. Previous efforts at directly dating deformation focused upon Rb-Sr dating of high Rb/Sr phases (e.g. Freeman *et al.*, 1997) and $^{40}Ar/^{39}Ar$ dating of white mica, amphibole and feldspar (e.g. Simon-Labric *et al.*, 2009). *In situ* $^{40}Ar/^{39}Ar$ dating of recrystallised micas by laser-heating techniques has successfully been applied to mylonites in low temperature conditions, but potential cm-scale mobility of Ar and excess-Ar may compromise successful thermochronology (Kelley, 2002, Mulch *et al.,* 2005). Texturally controlled Rb-Sr dating also has great potential, but is prone to resetting by post deformation fluid circulation (e.g. Wickman *et al.*, 1983) and isotopic disequilibrium on the thin-section scale (Frey *et al.*, 1976).

Uranium and thorium rich accessory phases, such as zircon and monazite, provide robust ages in many geological settings. Although mechanical modification of zircons in shear zones is relatively common, chemical modifications, and hence age resetting, are not (e.g. Wayne and Sinha, 1992, Moser *et al.,* 2009). To a lesser extent, U-Pb techniques have been successfully applied to dynamically

recrystallised titanite and monazite (Resor *et al.*, 1996; Storey *et al.*, 2004). Another accessory phase that is a prime target for geochronology in these environments is allanite, which is a rare earth element (REE) rich end-member of the epidote solid solution series ($[Ca,REE,Th]_2[Fe,Al]_3Si_3O_{12}[OH]$). The mineral is key to the storage and mobility of REE, Th and U (Hermann, 2002, Giéré and Sorensen, 2004), and offers geochronological information that can be linked with physico-chemical conditions (e.g., pressure, temperature conditions), based upon petrological observations. Allanite is also commonly found associated to monazite (Janots *et al.*, 2008). Epidote and clinozoisite generally surround allanite. As thermodynamic stabilities of these phases can be calculated, it is possible to make quantitative links between the timing of monazite/allanite/clinozoisite/epidote growth and *PT* conditions (e.g. Smye *et al.*, 2010).

A number of studies have reported on the textural and chemical relationships of allanite to rock-forming minerals, and on evidence of its stability in *PT*-space (Gregory *et al.*, 2009; Hermann, 2002; Janots *et al.*, 2008; Gregory *et al.*, 2012). Recent advances in allanite *in situ* U-Th-Pb dating yield reliable ages, despite the fact that allanite contains significant amounts of common Pb (Gregory *et al.*, 2007; Smith *et al.*, 2009; Darling *et al.*, 2012a). Whereas the petrology and geochemistry of allanite have been addressed repeatedly, little is known so far regarding the effects of deformation and recrystallization on allanite U-Th-Pb systematics (Cenki-Tok *et al.*, 2011).

Accordingly, we have investigated allanite-bearing samples from a greenschist facies shear zone of the Mont Blanc massif (MBM). The principal aims of this study are to: (a) investigate U-Th-Pb isotope systematics of synkinematic allanite using newly developed methods, taking into account the common-Pb composition reflecting the crystallization environment; (b) test whether allanite may be used to directly date the age of deformation and metasomatism.

Geological setting of the Mont Blanc shear zones

The MBM belongs to a suite of Variscan external crystalline massifs of the western Alps (Fig. 1). It is composed of gneisses and a granitic batholith that crystallized at 300 ± 3 Ma (Bussy and von Raumer, 1994). The general deformation pattern of the MBM consists of subvertical narrow (1 to 50

m) shear zones, arranged in a fan-like geometry, separated by low strain domains (100 to 500 m). Deformation, strain localization and associated upper greenschist facies metamorphism in the MBM have been considered Alpine in age (Rolland *et al.*, 2008).

The majority of shear zones are transpressive and form a complex network of anastomosing NNE-SSW (N40-60°E) and N-S (N160-20°E) components with sub-vertical stretching lineations (Fig. 1). These two groups of shear zones have a dextral and sinistral component, respectively, resulting in a NW-SE compression regime (Rossi *et al.*, 2005). In addition, domains of distinct mineral assemblages within shear zones can be recognized with an NW to SE zoning (Fig. 1). In the NW part, the dominant assemblage is epidote, quartz and muscovite, in the central part, phlogopite, chlorite and quartz are present, and in the SE part, phengite dominates.

Microstructure and petrology of the sample

This study focuses on a greenschist facies shear zone in the chlorite- and phlogopite-bearing domain (central domain of Fig. 1). This shear zone may be observed along-strike inside the Mont Blanc tunnel, emphasizing its regional 2-dimensional exposure. Lineations are subvertical and shear sense indicators reflect exclusively pure shear: i.e. horizontal shortening. The main mylonitic foliation is marked by chlorite, elongated K-feldspars and recrystallised quartz. Locally, phlogopite is present as larger crystals, and albite crystals occur in low strain parts of the sections of the shear zone. Thermodynamic phase equilibria indicate that shear zone recrystallisation occured at 0.51 ± 0.05 GPa and 400 ± 25 °C (Rolland *et al.*, 2003).

The contact between high-strain domains and low-strain granite pods is anastomosing and finger-like. In addition, a low Fe-content of fabric minerals is associated to high bulk-rock Mg/(Mg+Fe) values compared to the unaltered, undeformed granite. These evidence suggest a localized fluid alteration front associated with greenschist facies metamorphism. These are Mg-rich fluids percolating upwards in the core of the MBM, with high fluid/rock ratios (Rossi *et al.*, 2005).

Small (< 100 μm), newly crystallised REE-rich phases are parallel to, or occasionally overgrow, the main greenschist facies mylonitic foliation (Fig. 2). New aeschynite and elongate allanite crystals

are idioblastic and contain chlorite, albite and uraninite inclusions. In addition, there are clear differences in zoning, texture, composition and REE patterns between allanite in the host granite and in the shear zone (Rolland *et al.*, 2003), with the shear zone grains being homogeneous in major and REE elements composition (Fig. 3). These observations indicate that, texturally, allanite is not inherited, is in equilibrium with the mylonitic assemblage and therefore synkinematic.

Allanite dating methods

Laser ablation (LA)-ICP-MS U-Th-Pb isotope analyses were undertaken at the University of Portsmouth, using a New Wave 213 nm Nd:YAG laser coupled with an Agilent 7500cs ICP-MS. Analytical protocols and instrument conditions are described in detail by Darling et al. (2012a). Key points of the methodology are: (a) line-raster ablation, in order to minimize time-dependent elemental fractionation; (b) external normalisation to the zircon standard Plešovice (Slama *et al*, 2008); (c) the use of measured ^{204}Pb to correct for inherited common-Pb. Accuracy was monitored via analyses of the allanite reference materials Tara, Mucrone, BONA and SISS (von Blanckenburg, 1992; Gregory *et al.*, 2007; Cenki-Tok *et al.*, 2011), for each of which mean common-Pb corrected ^{208}Pb/^{232}Th ages are within uncertainty of reference values, with uncertainties of 0.5 to 1.5 percent (2σ; Table 1).

Pb-isotope measurements of albite and chlorite were undertaken in a polished block of the studied sample at the University of Bristol, using a New Wave Research 193 nm ArF Excimer laser coupled with a ThermoFinnigan Neptune multi-collector (MC)-ICP-MS. Analytical procedures followed those of Foster and Vance (2006) and Darling *et al.* (2012b). Sample measurements were normalised to the NIST 610 glass standard, and NIST 612 was used to monitor accuracy and precision, yielding mean ^{206}Pb/^{204}Pb, ^{207}Pb/^{204}Pb and ^{208}Pb/^{204}Pb values of 17.105 ± 0.008, 15.521 ± 0.006, and 37.035 ± 0.013 respectively (120 μm nominal beam diameter; n = 12; all uncertainties 2σ).

Allanite U-Th-Pb systematics

The results of allanite analyses are detailed in Table 2, and key points are summarised in Figure 4. The measured grains typically have high common-Pb contents, with measured ^{206}Pb/^{204}Pb and

$^{208}Pb/^{204}Pb$ varying from 32-184 and 60-474 respectively. A Tera-Wasserburg type concordia plot (Figure 4A) highlights the dominance of common-Pb. The regression has a poorly defined lower intercept of 21 ± 18 Ma (all uncertainties 2σ, unless otherwise stated), but interestingly has a very low y-intercept (0.41 ± 0.02), which reflects the $^{207}Pb/^{206}Pb$ composition of the common-Pb component (Tera and Wasserburg, 1972). This value is far removed from model terrestrial Pb isotope evolution curves (total $^{207}Pb/^{206}Pb$ range 0.84 to 1.11; Stacey and Kramers, 1975).

The isotopic composition of common-Pb in the metamorphic assemblage associated with allanite was further investigated via LA-MC-ICP-MS Pb isotope measurements of albite and chlorite from the same sample (Table 3). The measured albite crystals have highly radiogenic age-corrected Pb-isotope values, with weighted mean $^{206}Pb/^{204}Pb_i$, $^{207}Pb/^{204}Pb_i$ and $^{208}Pb/^{204}Pb_i$ values of 29.75 ± 0.39, 16.08 ± 0.12 and 46.05 ± 0.34 respectively (Figure 4B). These ratios were age corrected to 28.2 ± 2.6 Ma (the allanite Th-Pb isochron age; Fig. 4C) using measured $^{238}U/^{204}Pb$ and $^{232}Th/^{204}Pb$, although the magnitude of this correction is less than analytical uncertainty in albites due to low $^{238}U/^{204}Pb$ (<5.1) and $^{232}Th/^{204}Pb$ (<0.11). The single measurement of chlorite has $^{206}Pb/^{204}Pb_i$, $^{207}Pb/^{204}Pb_i$ and $^{208}Pb/^{204}Pb_i$ values within uncertainty of the albite mean. Two further analyses of chlorite were rejected due to ablation through Pb-rich inclusions and very low Pb concentration in one case. Importantly, these measured albite and chlorite values are within uncertainty of the initial $^{208}Pb/^{204}Pb$ and $^{206}Pb/^{204}Pb$ values provided by the Th-Pb and U-Pb isochrons (Fig. 4C-D). As suggested by textural and geochemical evidence, this indicates that allanite is in equilibrium with the mylonitic assemblage and offers new opportunities for accurate common-Pb correction.

Previous studies have advocated the use of assumed common-Pb compositions taken from model terrestrial Pb-isotope evolution curves (Stacey and Kramers, 1975), in order to correct Pb isotope signals for common-Pb in magmatic allanite (e.g. Gregory *et al.*, 2007). However, as shown in Figure 4E, Th/Pb ages corrected using a Stacey and Kramers (1975) composition are scattered and do not define a single age population. In contrast, when the measured Pb-isotope composition is used for correction, the data define a single age population, with a weighted mean of 29.44 ± 0.95 Ma (MSWD = 0.85; n = 30; Figure 4F). This value is within uncertainty of the Th-Pb isochron age for these data

(28.2 ± 2.6 Ma; Figure 5), which is independent of common-Pb correction. A necessary pre-requisite for this approach is that metamorphic allanite, chlorite and albite have equilibrated in the same common-Pb reservoir. In this case, this condition is fulfilled as i) allanites contain chlorite and albite inclusions; ii) initial $^{208}Pb/^{204}Pb$ from the allanite Th-Pb isochron (47.1 ± 2.3) is within error of the measured albite and chlorite values. There is minor variability in the initial Pb-isotope values of matrix phases that is greater than analytical precision. For example $^{206}Pb/^{204}Pb_i$ in albites range from 29.53 ± 0.28 to 30.40 ± 0.31. Further analyses are required to test the scale of Pb-isotope heterogeneity in such metamorphic systems, although this range of variability has a minor effect on calculated ages compared to uncertainty in measurement of ^{204}Pb in this study. In combination, this analysis of Pb-isotope systematics in allanite and other phases of the metamorphic assemblage provides confidence that the weighted-mean $^{208}Pb/^{232}Th$ age represents the best estimate of crystallization age of allanites in the studied sample.

Common Pb corrected $^{206}Pb/^{238}U$ ages are highly variable, and significantly older than Th-Pb ages. The slope of the U-Pb isochron (Fig. 4D) also provides a significantly older age (122 ± 32 Ma). Two lines of evidence suggest that the ^{238}U-^{206}Pb system is compromised by excess ^{206}Pb, either from ^{230}Th disequilibrium (e.g. Scharer, 1984; von Blankenburg, 1992), inherited radiogenic Pb from a U rich precursor (Romer and Siegesmund, 2003), labile ^{206}Pb from another source, or a combination of these factors: (1) the initial $^{206}Pb/^{204}Pb$ provided by the U-Pb regression is within uncertainty of the composition of albite and chlorite, suggesting variable levels of ^{206}Pb incorporation into different grains of allanite; (b) the low $^{207}Pb/^{206}Pb$ intercept of the Tera-Wasserburg regression (0.41 ± 0.02) compared to the albite-chlorite initial value (0.540 ± 0.014). Furthermore, there is a positive correlation between the Th/U ratios and $^{206}Pb/^{238}U$ ages of the allanite population, which suggests that U-Th fractionation during crystallization of allanite, causing initial ^{230}Th disequilibrium ($t_{1/2}$ = 75 kyr; e.g. Scharer, 1984; von Blankenburg, 1992), may be the dominant control on excess ^{206}Pb.

Discussion and conclusion

Significant improvement in understanding the petrology and geochemistry of allanite were made in the past decade (e.g. Janots *et al.*, 2008), but the effects of deformation and recrystallization on allanite U-Th-Pb systematics have as yet been little studied. A first attempt to test whether allanite may be used to infer the age of mylonitisation revealed that the mineral can be remarkably resistant to deformation in relatively dry conditions at eclogite facies due to mechanical shielding that prevents chemical equilibration (Cenki-Tok *et al.*, 2011). This study shows that new crystallisation of allanite may occur in shear zones associated to fluid flux, which can efficiently reset U-Th-Pb isotopic ratios. In the studied shear zone, allanite texturally belongs to the greenschist-facies assemblage. As shown by recent studies (e.g. Janots *et al.*, 2008), allanite is expected to be stable at these PT conditions (ca. 0.5 GPa and 400 °C, Rolland *et al.*, 2003).

The U-Th-Pb closure temperature of allanite is estimated to be above 700 °C (Heaman and Parrish, 1991), because i) allanite has been shown to remain closed to Pb loss and retain trace element and Sr-Nd isotope zonation during prolonged magmatic conditions (Oberli *et al.*, 2004; Gregory *et al.*, 2009); ii) in general zoning patterns developed in allanites during prograde metamorphic growth may be retained through peak conditions (Janots *et al.*, 2008). Due to the high closure temperature of allanite, the age of this study is interpreted as a crystallization age that records shear zone activation under greenschist facies conditions.

The allanite U-Th-Pb *in situ* isotope data from this study also highlights the importance of using measured Pb-isotope compositions for common-Pb, particularly in metamorphic rocks in which several processes may fractionate Th/Pb, U/Pb or Th/U. Measured albite and chlorite indicate that fluids associated with the metasomatic event (Rossi *et al.*, 2005) had highly radiogenic Pb-isotope compositions. Similar fluid compositions have already been recognised in this zone of the MBM (Marshall *et al.*, 1998). These were interpreted as being related to the emplacement of the Penninic Front that tapped fluid from deep crustal and mantle sources (Rossi *et al.*, 2005). Indeed, metasomatised rocks with similar $\delta^{13}C$ calcite ratios may also be found at the Penninic Front itself (Rossi *et al.*, 2005).

In summary, the mean Th-Pb age of 29.4 ± 1.0 Ma is taken as the crystallisation age of allanites in the studied shear zone, and hence the age of deformation and fluid percolation. In the SE domain of the MBM (Fig. 1), shear zones yielded younger ^{40}Ar-^{39}Ar crystallization ages (16 Ma; Rolland *et al.*, 2008). The diachroneity revealed by these two studies highlights a succession of previously unrecognized events in the MBM including: i) ductile deformation and fluid percolation at ca. 29 Ma ascribed to activation of the Penninic Front, which is also recognised further to the South in the Pelvoux Massif (Simon-Labric *et al.* 2009); ii) reactivation of the shear zones at 16-14 Ma is ascribed to the onset of exhumation in relation with the rotation of Apulia (Rolland *et al.*, 2012).

More generally, allanite may be found in a wide variety of lithologies (felsic, pelitic and mafic). It is a petrologically important mineral in greenschist to amphibolite grade rocks typical of the upper-mid crust, particularly when found together with monazite. As its closure temperature is well above these moderate mid-crustal temperatures (ca. 700 °C; Oberli, 1994), allanite ages in these environments are likely to record crystallization rather than cooling. Allanite therefore helps us understand the timing and rates of low to medium temperature processes, which are known to be difficult to date.

Acknowledgements

BCT thanks M. Engi and M. Rossi for discussion. Financial support from Swiss National Fund (Grants 200020-109637, 200021-117996/1, 200021-103479/1) is gratefully acknowledged. We thank C. Hetherington and two anonymous reviewers for their constructive comments as well as Klaus Mezger for editorial handling.

References

Bussy, F. and von Raumer, J.F., 1994. U-Pb geochronology of Paleozoic magmatic events in the Mont Blanc crystalline massif, Western Alps. *Schweizerische Mineralogische Und Petrographische Mitteilungen*, **74**, 514-515.

232 Cenki-Tok, B., Oliot, E., Rubatto, D., Berger, A., Engi M., Janots, E., Thomsen, T.B., Manzotti, P.,
233 Regis, D., Spandler, C., Robyr, M., and Goncalves, P., 2011. Preservation of Permian allanite
234 within an Alpine eclogite facies shear zone at Mt Mucrone, Italy: Mechanical and chemical
235 behavior of allanite during mylonitization. *Lithos*, **125**, 40-50.

236 Darling, J.R., Storey, C.D. and Engi, M., 2012a. Allanite U-Th-Pb geochronology by laser ablation
237 ICP-MS. *Chemical Geology*, **292-293**, 103-115.

238 Darling, J.R., Storey, C.D., Hawkesworth, C.J. and Lightfoot, P.C., 2012b. *In situ* Pb isotope analysis
239 of Fe–Ni–Cu sulphides by laser ablation multi-collector ICP-MS: New insights into ore
240 formation in the Sudbury impact melt sheet. *Geochimica et Cosmochimica Acta,* **99**, 1-17.

241 Foster, G.L. and Vance, D., 2006. Negligible glacial-interglacial variation in continental chemical
242 weathering rates. *Nature*, **444**, 918-921.

243 Freeman, S.R., Inger, S., Butler, R.W.H., and Cliff, R.A., 1997. Dating deformation using Rb-Sr in
244 white mica. Greenschist facies deformation ages from the Entrelor shear zone, Italian Alps:
245 *Tectonics*, **16-1**, 57-76.

246 Frey, M., Hunziker, J.C., O'Neil, J.R. and Schwander, H.W., 1976. Equilibrium-disequilibrium
247 relations in the Monte Rosa granite, Western Alps: petrological, Rb-Sr and stable isotope data.
248 *Contribution to Mineralogy and Petrology*, **55**, 147-179.

249 Gieré, R. and Sorensen, S.S., 2004. Allanite and other REE-rich epidote-group minerals. *Reviews in*
250 *Mineralogy and Geochemistry,* **56**, 431–493.

251 Gregory, C.J., Rubatto, D., Allen, C.M., Williams, I.S., Hermann, J., and Ireland, T., 2007. Allanite
252 micro-geochronology: A LA-ICP-MS and SHRIMP U-Th-Pb study. *Chemical Geology*, **245**,
253 162-182.

254 Gregory, C.J., Buick, I.S., Hermann, J. and Rubatto, D., 2009. Mineral-scale Trace Element and
255 UThPb Age Constraints on Metamorphism and Melting during the Petermann Orogeny
256 (Central Australia). *Journal of Petrology*, **50(2)**, 251-287.

257 Gregory, C.J., Rubatto, D., Hermann, J., Berger, A. a,d Engi, M., 2012. Allanite behaviour during
258 incipient melting in the southern Central Alps. *Geochimica Cosmochimica Acta*, **84**, 433-458.

259 Heaman, L. and R. Parrish, 1991, "U-Pb Geochronology of Accessory Minerals," chapter 3 in L.
260 Heaman and J.N. Ludden, *Applications of Radiogenic Isotope Systems to Problems in*
261 *Geology*, Short Course Handbook, v. 19.

262 Hermann, J., 2002. Allanite: thorium and light rare earth element carrier in subducted crust. *Chemical*
263 *Geology*, **192 (3-4)**.

264 Jaffey, A., Flynn, K., Glendenin, L., Bentley, W., Essling, A., 1971. Precision Measurement of Half-
265 Lives and Specific Activities of 235U and 238U. Phys. Rev. C 4, 1889-1906

266 Janots, E., Engi, M., Berger, A., Allaz, J., Schwarz, J.-O., and Spandler, C., 2008. Prograde
267 metamorphic sequence of REE minerals in pelitic rocks of the Central Alps: implications for
268 allanite-monazite-xenotime phase relations from 250 to 610 degrees C. *Journal of*
269 *Metamorphic Geology*, **26 (5)**, 509-526.

270 Kelley, S., 2002. Excess argon in K-Ar and Ar-Ar geochronology. *Chemical Geology*, **188**, 1-22.

271 Marshall, D., Pfeifer, H.-R., Hunziker, J.C. and Kirschner, D., 1998. A pressure-temperature-time path
272 for the NE Mont-Blanc massif: Fluid-inclusion, isotopic and thermobarometric evidence.
273 *European Journal of Mineralogy*, **10**, 1227-1240.

274 Moser, D.E., Davis, W.J., Reddy, S.M., Flemming, R.L. and Hart, R.J., 2009. Zircon U-Pb strain
275 chronometry reveals deep impact-triggered flow. *Earth and Planetary Sciences Letters*, **277**,
276 73-79.

277 Mulch, A., Cosca, M.A., Andersen, A. and Fiebig, J., 2005. Time scales of deformation and
278 exhumation in extensional detachement systems determined by high-spatial resolution *in situ*
279 UV-laser $^{40}Ar/^{39}Ar$ dating. *Earth and Planetary Sciences Letters*, **233**, 375-390.

280 Oberli, F., Meier, M., Berger, A., Rosenberg, C., and Giere, R., 2004. U–Th–Pb and Th-230/U-238
281 disequilibrium isotope systematics: precise accessory mineral chronology and melt evolution
282 tracing in the Alpine Bergell intrusion. *Geochimica Cosmochimica Acta*, **68**, 2543–2560.

283 Petrik, I., Broska, I., 1994. Petrology of 2 granite types from the Tribec mountains, western
284 Carpathians — an example of allanite (+ magnetite) versus monazite dichotomy. Geological
285 Journal 29 (1), 59–78.

286 Resor, P., Chamberlain, K.R., Frost, C.D., Frost, B.R., and Snoke, A.W., 1996. Direct dating of
287 deformation; U-Pb age of syndeformational sphene growth in the Proterozoic Laramie Peak
288 shear zone. *Geology*, **27 (7)**, 623-626.

289 Rolland, Y., Cox, S., Boullier, A.-M., Pennacchioni, G., and Mancktelow, N.S., 2003. Rare earth and
290 trace element mobility in mid-crustal shear zones: insights from the Mont Blanc Massif
291 (Western Alps). *Earth and Planetary Science Letters*, **214**, 203-219.

292 Rolland, Y., Rossi, M., Cox, S.F., Corsini, M., Mancktelow, N., Pennacchioni, G., Fornari, M., and
293 Boullier, A.M., 2008. $^{40}Ar/^{39}Ar$ dating of synkinematic white mica: insights from fluid-rock
294 reaction in low-grade shear zones (Mont Blanc Massif) and constraints on timing of
295 deformation in the NW external Alps. *Geological Society, London, Special Publications*, **299**,
296 293-315.

297 Rolland, Y., Lardeaux, J.-M. and Jolivet, L., 2012. Deciphering orogenic evolution. *Journal of*
298 *Geodynamics*, **56-57**, 1-6.

299 Romer, R. L., and Siegesmund, S., 2003. Why allanite may swindle about its true age. *Contributions*
300 *to Mineralogy and Petrology*, **146**, 3, 297-307.

301 Rossi, M., Rolland, Y., Vidal, O. and Cox, S.F., 2005. Geochemical variations and element transfer
302 during shear-zone development and related episyenites at middle crust depths: insights from
303 the Mont Blanc granite (French-Italian Alps). *Geological Society, London, Special*
304 *Publications*, **245**, 373-396.

305 Schärer, U., 1984. The effect of initial ^{230}Th disequilibrium on young U-Pb ages: the Makalu case,
306 Himalaya. *Earth and Planetary Science Letters*, **67**, 191-204.

307 Simon-Labric, T., Rolland Y., Dumont, T., Heymes, C., Authemayou, M., Corsini, M., and Fornari.,
308 M., 2009. $^{40}Ar/^{39}Ar$ dating of Penninic Front tectonic displacement (W Alps) during the
309 Lower Oligocene (31-34 Ma). *Terra Nova*, **21**, 127-136.

310 Slama, J., Košler, J., Condon, D.J., Crowley, J.L., Gerdes, A., Hanchar, J.M., Horstwood, M.S.A.,
311 Morris, G.A., Nasdala, L., Norberb, N., Schaltegger, U., Schoene, B., Tubrett, M.N., and
312 Whitehouse, M.J., 2008. Plešovice zircon - A new natural reference material for U-Pb and Hf
313 isotopic microanalysis. *Chemical Geology*, **249**, 1-35.

314 Smith, M.P., Storey, C., Jeffries, T. and Ryan, C., 2009. *In situ* U-Pb and trace element analysis of
315 accessory minerals in the Kiruna district, Norrbotten, Sweden: New constraints on the timing
316 and origin of mineralization. *Journal of Petrology*, **50 (11)**, 2063-2094.

317 Smye, A.J., Greenwood, L.V. & Holland, T.J.B. (2010). Garnet-chloritoid-kyanite assemblages:
318 eclogite facies indicators of subduction constraints in orogenic belts. *Journal of Metamorphic*
319 *Geology,* **28**, 753-768.

320 Stacey, J.S., and Kramers, J.D., 1975. Approximation of terrestrial lead isotope evolution by a two
321 stage model. *Earth and Planetary Science Letters*, **26**, 207-221.

322 Storey, C.D., Brewer, T.S., and Parrish, R.R., 2004. Late-Proterozoic tectonics in northwest Scotland:
323 one contractional orogeny or several?. *Precambrian Research*, **134**, 227-247.

324 Tera, F., and Wasserburg, G., 1972. U-Th-Pb systematics in three Apollo 14 basalts and the problem
325 of initial Pb in lunar rocks. *Earth and Planetary Science Letters*, **14**, 281-304.

326 Wayne, D.M., and Sinha, A.K., 1992. Stability of zircon U-Pb systematics in a greenschist-grade
327 mylonite – An example from the Rockfish valley fault zone, Central Virginia, USA. *Journal*
328 *of Geology*, **100 (5)**, 593-603.

329 Wickman, F.E., Aberg, G., and Levi, B., 1983. Rb-Sr dating of alteration events in granitoids.
330 *Contribution to Mineralogy and Petrology*, **83**, 358-362.

von Blanckenburg, F., 1992. Combined high-precision chronometry and geochemical tracing using accessory minerals: applied to the Central-Alpine Bergell intrusion (central Europe). *Chemical Geology*, **100**, 19-40.

Figure and table caption :

Figure 1: Simplified geological map and cross-section (without vertical exaggeration) of the Mont Blanc Massif with main structural features and mineral assemblages (modified from Rolland *et al.*, 2008). UTM Coordinates of studied sample : (WGS84): N5084.005; E343.502.

Figure 2: Plane polarized light microphotographs of allanite crystals within the studied greenschist facies shear zone.

Figure 3: REE versus Al diagram (after Petrík *et al.*, 1995), showing the compositions of allanites measured by electron microprobe in this study.

Figure 4: Allanite U-Th-Pb ICP-MS isotope data for sample C33. (A): Tera-Wasserburg plot of allanite analyses uncorrected for common Pb. (B): Age corrected Pb isotope compositions of albites and chlorite. (C) Th-Pb and (D) U-Pb isochron plots for the allanite analyses of this study. A calculated U-Pb isochron corresponding to an age of 30 Ma, and using the albite and chlorite measured Pb isotope composition, is also shown in B for comparison. Data are not corrected for common-Pb. All uncertainties are at the 95% confidence level. (E)-(F): Common-Pb corrected Pb/Th ages of allanites, showing the importance of using measured Pb isotope ratios for common Pb correction.

Table 1: Summary of allanite U-Th-Pb isotope data for reference materials. The reference ages were measured by Thermal Ionisation Mass Spectrometry (TIMS; von Blanckenburg, 1992) or Sensitive High Resolution Ion Microprobe (SHRIMP; Gregory *et al.*, 2007; Cenki-Tok *et al.*, 2011).

Table 2: Allanite U-Th-Pb isotope data for Mont Blanc sample C33

356 Table 3: Laser ablation MC-ICP-MS Pb isotope data

357

358

359

360

Table 1:Summary of allanite U-Th-Pb isotope data for reference materials

All analyses at the School of Earth and Environmental Science, University of Portsmouth, United Kingdom

			Mean ratios and common-Pb contents										Tera-Wasserburg Regression		Mean common-Pb corrected ages						
Material	No. analyses	Raster (μm)[1]	$^{206}Pb/^{204}Pb$	1σ	$^{208}Pb/^{204}Pb$	1σ	^{206}com %	1σ	^{207}com %	1σ	^{208}com %	1σ	L. Intercept (Ma)	1σ abs	$^{206}Pb/^{238}U$	2σ abs	$^{208}Pb/^{232}Th$	**2σ abs**	Ref. Age (Ma)	Notes	Ref.
SISS	4	25 x 40	31	2	57	4	59	3	93	4	38	3	48	33	35.3	2.5	**32.9**	**2.2**	*31.5 ± 0.35*	*Large ^{206}Pb excess*	*von Blanckenburg (1992)*
BONA	4	25 x 40	24	4	219	50	79	14	96	5	18	4	82	25	45	35	**31.0**	**0.7**	*30.1 ± 0.4*	*Large ^{206}Pb excess*	*von Blanckenburg (1992)*
Tara	6	25 x 40	459	625	19232	32090	16	15	65	60	1	1	420	14	424	11	**416.4**	**3.4**	*414.9 ± 3.3*		*Gregory et al., (2007)*
Mucrone	4	25 x 40	90	40	588	150	23	9	76	8	7	2	265	34	316	55	**286.6**	**5.5**	*287 ± 7*		*Cenki-Tok et al. (2011)*

Table 2: Allanite U-Th-Pb isotope data for Mont Blanc sample C33

All analyses at the School of Earth and Environmental Science, University of Portsmouth, United Kingdom

C33 - Mont Blanc					Common-Pb contents[2]							Data for Tera-Wasserburg plot[3]							Common-Pb corrected ages[4]			
Identifier	Raster (μm)[1]	^{204}Pb cps	Th /U	1σ %	^{206}Pb /^{204}Pb	1σ %	^{208}Pb/ ^{204}Pb	1σ %	^{206}com %	^{207}com %	^{208}com %	^{238}U/ ^{206}Pb	1σ abs	^{207}Pb/ ^{206}Pb	1σ abs	^{208}Pb/ ^{206}Pb	^{208}Pb/ ^{232}Th	1σ %	^{206}Pb/ ^{238}U	2σ abs	^{208}Pb/ ^{232}Th	2σ abs
Au16C07	25 x 40	81	25	4	43	8	79	8	70	99	58	15.4	0.5	0.37	0.02	1.8	0.0036	2.3	127	36	31.3	6.5
Au16C08	25 x 40	64	16	6	45	7	73	6	67	97	63	16.7	1.3	0.37	0.02	1.6	0.0049	2.9	125	65	37.6	9.2
Au16C09	25 x 40	76	15	7	42	5	70	4	72	96	66	18.8	1.1	0.39	0.02	1.6	0.0048	3.2	97	44	33.9	9.1
Au16C10	25 x 40	85	16	6	41	13	72	10	74	100	64	20.4	0.5	0.39	0.01	1.7	0.0045	2.2	82	23	33.1	7.5
Au16C11	25 x 40	65	35	4	41	13	74	10	73	96	62	12.6	0.4	0.40	0.02	1.8	0.0036	2.5	136	43	28.3	6.5
Au16C12	25 x 40	125	21	5	43	11	70	4	71	99	66	11.9	0.3	0.38	0.01	1.6	0.0049	1.7	158	41	34.7	7.7
Au17c05	25 x 40	45	71	5	48	17	103	8	62	84	45	12.7	0.5	0.40	0.03	2.1	0.0024	2.3	188	54	27.1	4.3
Au17c06	25 x 40	73	36	6	55	16	108	8	55	78	43	20.9	0.5	0.38	0.01	1.9	0.0027	1.5	137	27	31.1	4.3
Au17c07	25 x 40	36	34	4	39	18	70	9	77	100	66	13.6	0.9	0.39	0.03	1.7	0.0040	3.6	111	66	28.1	8.0
Au17c08	25 x 40	15	52	5	184	7	474	5	16	17	10	31.5	1.9	0.39	0.03	2.5	0.0016	3.9	169	26	29.5	2.7
Au17c09	25 x 40	42	62	5	54	11	96	9	56	80	48	10.5	0.5	0.37	0.03	1.7	0.0028	4.0	266	77	29.7	6.2
Au17c10	25 x 40	29	53	5	41	19	87	9	74	94	53	14.7	0.7	0.42	0.03	2.1	0.0027	3.7	114	50	25.9	5.8
Au17c11	25 x 40	19	36	6	72	8	164	6	42	63	28	29.2	3.6	0.35	0.02	2.2	0.0022	2.2	127	56	31.7	3.3
Au17c12	25 x 40	35	64	5	51	13	103	10	59	80	45	13.1	0.6	0.40	0.03	2.0	0.0025	1.9	199	57	27.7	4.2
Au17c13	25 x 40	19	71	5	46	16	108	12	65	79	43	16.1	2.4	0.43	0.03	2.3	0.0021	7.2	140	123	24.0	6.8
Au17c14	25 x 40	81	60	5	54	14	112	7	56	78	41	14.0	0.4	0.38	0.02	2.0	0.0025	1.7	202	42	29.9	4.1
Au17c15	25 x 40	51	32	5	42	14	71	7	71	99	64	15.3	0.4	0.39	0.02	1.7	0.0035	2.3	119	33	25.2	5.8
Au17c16	25 x 40	34	38	5	40	17	73	9	76	100	63	14.2	0.7	0.39	0.02	1.8	0.0036	3.3	110	53	26.9	6.9
Au17d05	25 x 40	58	43	5	39	12	74	6	71	96	57	15.0	0.4	0.39	0.02	2.0	0.0033	2.8	125	35	28.9	6.1
Au17d06	25 x 40	52	63	5	32	18	70	10	77	98	54	13.1	0.5	0.42	0.03	2.3	0.0030	2.1	111	46	27.7	5.1
Au17d07	25 x 40	56	36	6	39	10	72	6	68	84	56	17.6	0.9	0.43	0.03	1.9	0.0033	2.8	117	44	28.7	6.1
Au17d08	25 x 40	15	72	5	98	22	184	16	71	99	48	11.3	0.6	0.38	0.02	1.9	0.0031	2.6	166	66	32.9	5.7
Fe14d05	30 x 45	121	35	4	39	4	72	2	76	100	64	12.0	0.3	0.41	0.01	2.1	0.0038	1.8	130	39	27.5	5.9
Fe14d06	30 x 45	199	7	7	43	3	60	2	69	98	76	26.1	0.7	0.37	0.02	1.6	0.0067	2.2	78	20	32.1	9.4
Fe14d07	30 x 45	13	24	4	41	17	75	9	72	99	62	19.2	1.3	0.39	0.03	2.1	0.0034	3.7	93	50	26.7	7.1
Fe14d08	30 x 45	29	32	5	62	13	127	7	48	69	36	22.0	0.5	0.37	0.01	2.3	0.0024	1.8	152	26	30.5	3.8
Fe14d09	30 x 45	65	29	5	39	9	65	4	76	99	71	10.4	0.3	0.41	0.01	1.9	0.0050	2.3	148	51	29.7	7.8
Fe14d10	30 x 45	19	29	5	41	18	71	8	72	99	65	12.0	0.4	0.39	0.02	2.0	0.0043	2.2	150	45	30.5	7.1
Fe14d11	30 x 45	26	35	6	50	14	89	7	60	95	52	13.2	0.5	0.37	0.02	2.1	0.0033	2.1	192	50	31.9	5.7
Fe14d12	30 x 45	53	14	4	44	9	73	4	68	96	63	28.5	1.9	0.38	0.01	1.9	0.0035	2.4	71	33	25.9	5.9

[1] Nominal beam diameter and line raster length.
[2] Ratio of common-Pb to total Pb signal, given as percentage.
[3] Data not corrected for common-Pb.
[4] Common-Pb corrected using measured Pb isotope ratios from feldspars and chlorites.
Decay constants of Jaffey et al (1971) used

Table 3: Laser ablation MC-ICPMS Pb isotope data

Analyses at the Department of Earth Sciences, University of Bristol, United Kingdom

				Measured Ratios										U-Th-Pb data[3]					Age corrected ratios[4]					
Identifier	Phase	Beam (μm)[1]	Pb_{total} (V)[2]	$^{206}Pb/^{204}Pb$	2σ abs	$^{207}Pb/^{204}Pb$	2σ abs	$^{208}Pb/^{204}Pb$	2σ abs	$^{207}Pb/^{206}Pb$	2σ abs	$^{208}Pb/^{206}Pb$	2σ abs	Pb (ppm)	$^{238}U/^{204}Pb$	2σ abs	$^{232}Th/^{204}Pb$	2σ abs	$^{206}Pb/^{204}Pb$	2σ abs	$^{207}Pb/^{204}Pb$	2σ abs	$^{208}Pb/^{204}Pb$	2σ abs
C33_01	Albite	120	0.26	29.88	0.23	16.18	0.10	46.28	0.31	0.542	0.002	1.550	0.004	1.5	5.1	0.3	0.09	0.01	29.63	0.23	16.16	0.10	46.27	0.31
C33_02	Albite	120	0.26	29.92	0.23	16.11	0.12	46.18	0.34	0.539	0.002	1.544	0.003	1.7	4.1	0.2	0.10	0.01	29.72	0.23	16.10	0.12	46.18	0.34
C33_03	Albite	90	0.18	29.78	0.28	16.11	0.15	46.02	0.44	0.541	0.001	1.547	0.001	2.1	4.9	0.3	0.11	0.01	29.53	0.28	16.10	0.15	46.02	0.44
C33_04	Albite	90	0.14	29.87	0.36	15.88	0.19	45.48	0.55	0.532	0.001	1.524	0.002	2.8	5.0	0.3	0.09	0.01	29.62	0.36	15.87	0.19	45.48	0.55
C33_05	Albite	120	0.22	30.64	0.31	16.03	0.14	45.82	0.41	0.523	0.002	1.497	0.004	1.6	4.9	0.3	0.10	0.01	30.40	0.31	16.02	0.14	45.82	0.41
C33_06	Chlorite	120	0.18	31.65	0.39	16.20	0.19	46.65	0.56	0.512	0.001	1.475	0.002	1.1	45.0	2.6	5.00	0.28	29.43	0.39	16.09	0.19	46.57	0.56

[1] Nominal beam diameter

[2] Total Pb signal in volts, using 10^{11} Ω resistors for all isotopes.

[3] U-Th-Pb concentrations and ratios measured at the University of Bern, utilising a GeoLas 193nm excimer laser coupled with a Elan DRC-e (quadrupole) ICPMS. Analyses were normalised to NIST SRM 610, and NIST SRM 612 was used as a consistency standard. ^{29}Si was used as an internal standard.

[4] Pb isotope ratios corrected for in-growth of radiogenic Pb to 30 Ma. Note that the magnitude of correction is small compared to analytical uncertainties on Pb isotope ratio measurements.

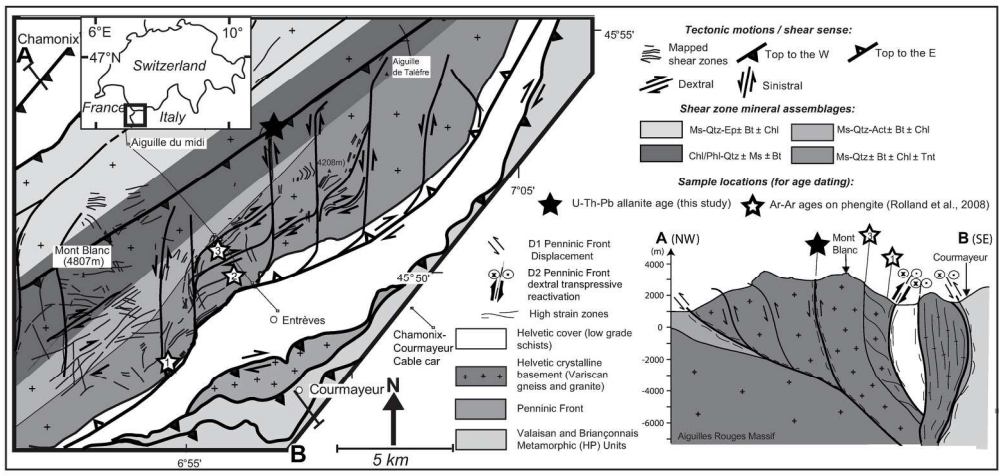

Figure 1: Cenki-Tok et al.

187x167mm (300 x 300 DPI)

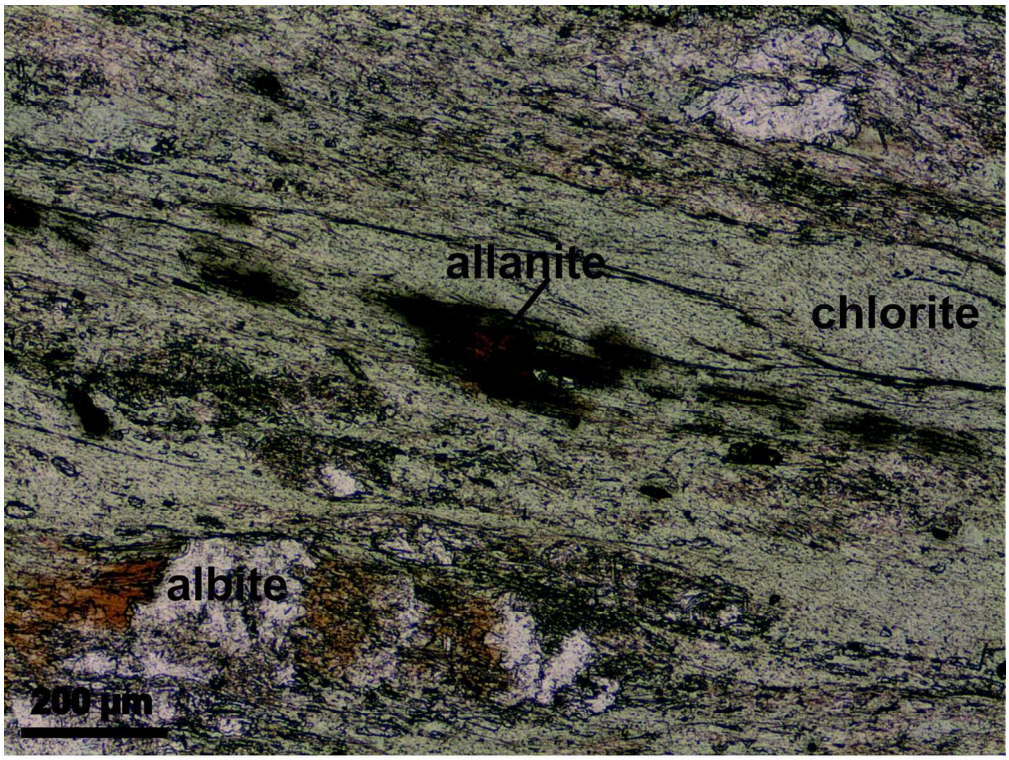

Figure 2: Cenki-Tok et al.

136x137mm (300 x 300 DPI)

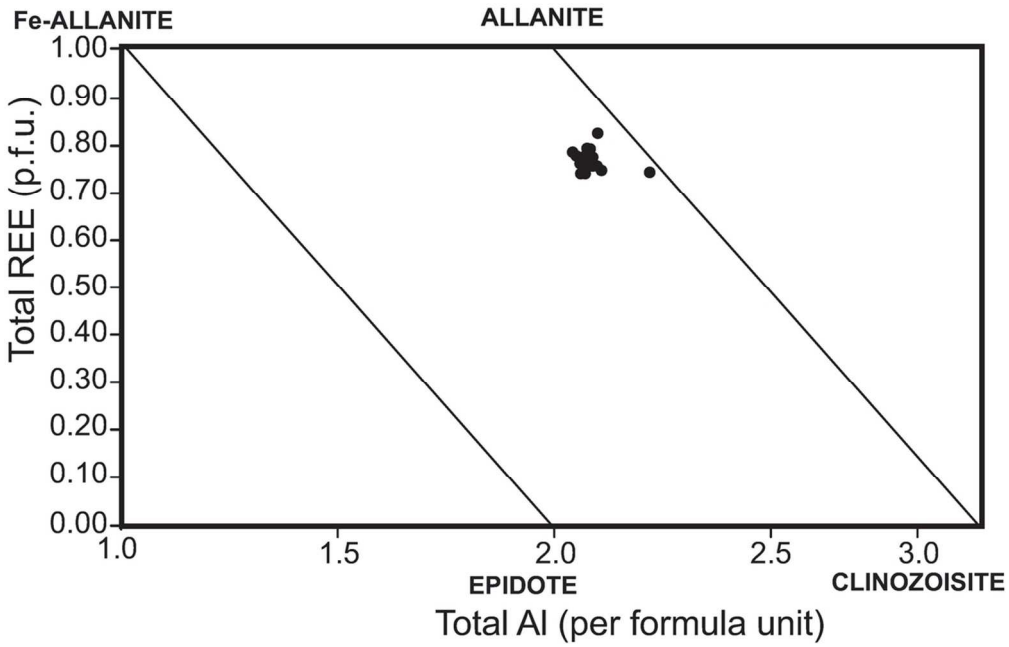

Figure 3: Cenki-Tok et al.

106x80mm (300 x 300 DPI)

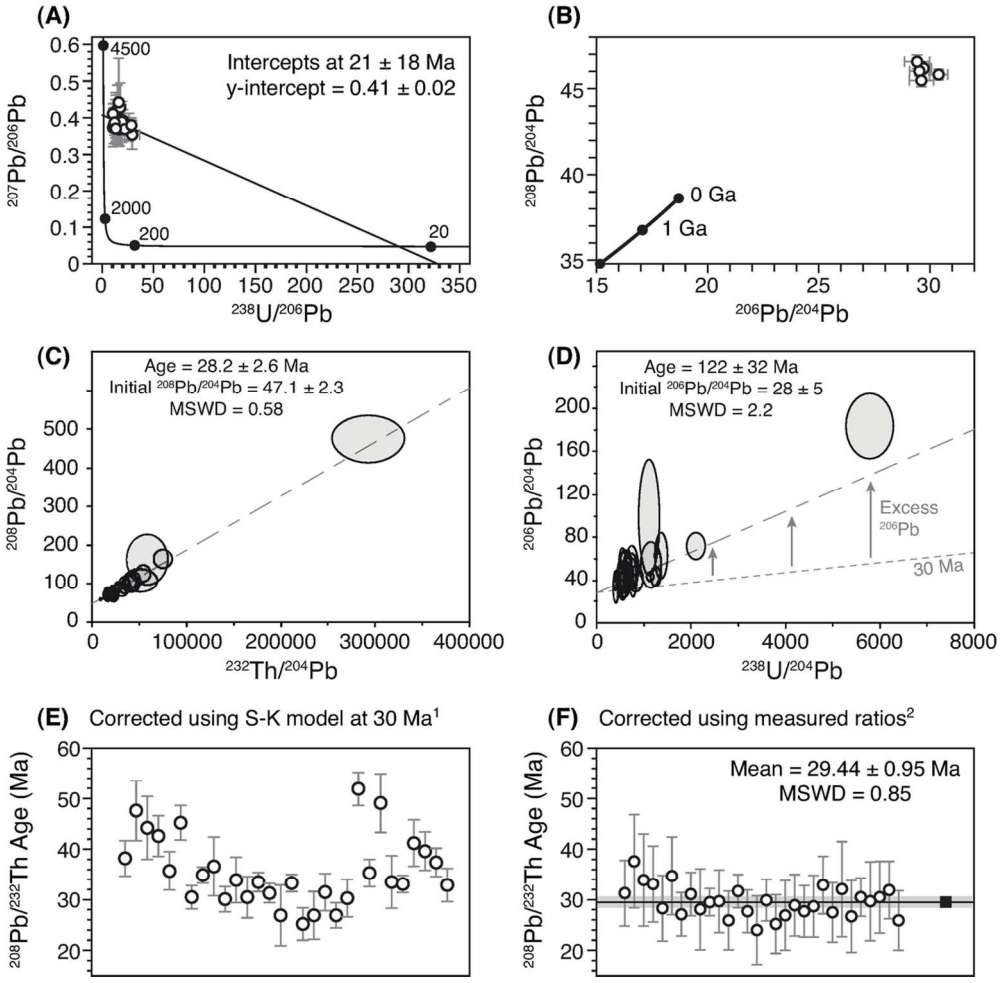

113x110mm (300 x 300 DPI)